PCCP

Accepted Manuscript

ROYAL SOCIETY OF CHEMISTRY

www.rsc.org/pccp

Cite this: DOI: 10.1039/c0xx00000x

www.rsc.org/xxxxxx

ARTICLE TYPE

Saddle-Shaped Porphyrins for Dye-Sensitized Solar Cells: New Insight into the Relationship between Nonplanarity and Photovoltaic Properties

Hashem Shahroosvand[a*], Saeed Zakavi[b] , Ahmad Sousaraei[a] , Mortaza Eskandari[a]

[a] Chemistry Department, University of Zanjan, Zanjan, Iran.

[b] Department of Chemistry , Institute for Advanced Studies in Basic Sciences, Gavazang, Zanjan, Iran.

Received (in XXX, XXX) XthXXXXXXXXX 20XX, Accepted Xth XXXXXXXXX 20XX
DOI: 10.1039/b000000x

We report on the theoretical and experimental studies of the new dye-sensitized solar cells functionalized with 5, 10, 15, 20-tetrakis(4-carboxyphenyl) porphyrin zinc(II) complexes bearing 2 and 8 bromo substituents at the β positions. In agreement with the results of TD-DFT calculation, the absorption maxima of di- and octa-brominated Zn(II) complexes, $ZnTCPPBr_2$ and $ZnTCPPBr_8$, exhibited large red-shifts compared to that of the non-brominated free base porphyrin (H_2TCPP). Furthermore, DFT calculations showed that the higher stabilization of the LUMO levels relative to the HOMO ones makes the HOMO–LUMO gaps of the brominated Zn-porphyrins models smaller compared to that of the nonbrominated counterparts, which explains the red shifted Soret and Q bands of the brominated compounds. Solar cells containing the new saddle-shaped porphyrins were subjected to analysis by a photovoltaic calibration laboratory to determine their solar to electric energy conversion. In this regard, we found that the overall conversion efficiency of $ZnTCPPBr_8$ adsorbed on TiO_2 nanocrystalline films being 5 times as large as that of $ZnTCPPBr_2$ adsorbed on the same films. The effect of increasing number of Br groups on the photovoltaic performance of the complexes was compared to results of computational methods by ab initio DFT molecular dynamics simulations and quantum dynamics calculations of electronic relaxation to investigate the interfacial electron transfer (IET) in $TCPPBr_x/TiO_2$-anatase nanostructures. Better IET for the $ZnTCPPBr_8$ compared to $ZnTCPPBr_2$, and for H_2TCPP was evaluated from interfacial electron transfer simulation (IETs). IET results indicate that electron injection in $ZnTCPPBr_8$-TiO_2 (τ = 25 fs) can be up to 5 order of magnitude faster than $ZnTCPPBr_2$-TiO_2 (τ = 125 fs). Both experimental and theoretical results demonstrate that the increasing of the number of bromo substituent at the β-pyrrole position of the porphyrin macrocycle created a new class of porphyrin DSSC, which exhibits a remarkable increase in photovoltaic performance than non- brominated porphyrins.

1. Introduction:

The sensitization of semiconductors with a significant number of dyes for light harvesting has been investigated over the last 25 years for the development of efficient solar cells.[1] Porphyrin sensitizers were among the first examined natural types of dyes, and to this day they continue to be some of the most frequently studied sensitizers. [2-5] Recently, a breakthrough has been achieved in porphyrin-sensitised sloar cell field when a record efficiency of 13% has been reported using a single push– pull porphyrin dye SM315 with cobalt (II/III)-based redox electrolyte. [6] In this regards, a widely used approach is to modify the porphyrins in the hope of increasing the charge-injection and light-harvesting efficiencies. One of the most appealing aspects of these methods is that a wide variety of functionalized porphyrins with different spectroscopic properties can now be synthesized.[7] Meanwhile, extension the light-harvesting region into the near-infra-red (NIR) is a one of the main strategies for improvement of the efficiency of a DSSC. [8] The free-base and zinc derivatives of the meso-benzoic acid substituted porphyrins (TCPP) are one of the most widely studied dyes due to their appropriate LUMO and HOMO energy levels.[9] However, the nearly orthogonal orientation of the meso aryl substituent with respect to the porphyrin mean plane may limit injection from ZnTCPP. [8] In contrast, the decreased dihedral angles between the aryl substituent and the porphyrin mean plane caused by the introduction of halogen group at the β- position of ZnTCPP, might allow more efficient direct charge injection from the porphyrin moiety to the semiconductor surface as well as the pushing of the Soret band to higher wavelengths, accounting for the higher performance of halogenated Zn-porphyins.[11] In particular, the modification of ZnTCPP by substitution at the β-positions with halogen atoms decreases the splitting between the key filled or empty orbitals, and leads to the enhancement of the red-absorbing Soret and Q bands. [12, 13] The four orbital model states [14] that the degeneracy of the two e_g LUMOs and the near-degeneracy of the a_{2u} HOMO and a_{1u} HOMO-1 causes strong configuration interaction between the $(a_{2u}\ e_g)^1$ and $(a_{1u}\ e_g)^1$ excited states of e_u symmetry. In addition, the electron-withdrawing substituent makes the macrocycle more electron deficient and consequently more stable towards oxidative degradation. Among the known β-pyrrole halogenated porphyrins, β-pyrrole brominated porphyrins have been a subject of intense research, because of their synthetic ease and the fact that the number of bromo substituent can be controlled with a high degree of certainty. [15]

The Soret and visible absorption bands of porphyrins have been shown to be highly sensitive to distortion of the porphyrin ring caused by peripheral substitution of the aromatic macrocycle.[16, 17] Hence, one can quantitatively probe the porphyrin geometry by measuring wavelengths and molar absorptivities of each ($TPPBr_x$)Zn derivative as a function of the number of Br groups introduced on the macrocycle. The above discussion clearly demonstrates the importance of β-pyrrole halogenated porphyrins from both fundamental and applied points of view. [18]

In fact, β-pyrrole halogenated porphyrins are a kind of a "missing link in the family tree" represented by porphyrin sensitizers in DSSC application. Therewith, understanding the photophysics of porphyrins attached to semiconductor surfaces is essential for the design of β-pyrrole halogenated porphyrins for solar energy conversion. [19] In this area, there is still considerable controversy about the time scale and nature of the primary electron-transfer process in dye sensitized TiO_2 electrodes, revealing that nuclear motion cannot be the rate-determining factor in the underlying interfacial electron-transfer mechanisms. Therefore, it seems essential to combine experimental studies with realistic theoretical simulations to develop a comprehensive understanding of the underlying electron-transfer dynamics. [20]

The efficiency of photon-to-current conversion thus relies upon optimal conditions for the underlying electron transfer mechanism as well as on the rational design of dyes and linker photosensitizes. Thus in focusing on photoinjection mechanisms from the excited electronic states of new β-pyrrole brominated porphyrins sensitized solar cells, this study examines the process of electron injection through and its application to design of efficient photo transductive devices.

Here, we focus on TiO_2 surfaces modified by zinc porphyrins attached to the surface by carboxylate linkers. Emphasis has been given to the characterization of the electronic excitations and injection time scales as determined by the number of the bromine atom at the β-pyrrole position of carboxylated porphyrin. The simulation results described in this paper show the first direct evidence of an electron-injection mechanism and the relation of substituent atoms in porphyrins and time-dependent charge distribution during the time relaxation dynamics. The interfacial electron-transfer involves an ultrafast (τ =25-120 fs) electron-transfer event that localizes the charge on the Ti^{4+} surface ions next to the adsorbate molecule.

2. Experimental:

2.1 Material and Instruments. All chemicals and solvents were purchased from Merck & Aldrich and used without further purification. IR spectra were recorded on a Perkin-Elmer 597 spectrometer ^{1}H-NMR spectra were recorded by use of a Bruker 250 MHz, spectrometer. The molecular and electronic structure calculations were performed with density functional theory (DFT) using the Gaussian 03(G03) program package. The B3LYP functional [21] with the LANL2DZ basis set was carried out. All geometry optimizations were performed in either C1 or C2 symmetry with subsequent frequency analysis to show that the structures are at the local minima on the potential energy surface. In addition, our calculations were performed in THF solvent. The electronic orbitals were visualized using GaussView 3.0.

2.2 Model system. The model system is initially defined according to the unrelaxed anatase nanostructure depicted in Figure 1. The nanostructure is composed of 32 [TiO_2] units, with bond lengths and angles initially defined according to the literature. [22] The largest conformational changes involve geometry rearrangements associated with the Ti^{4+} and O^{2-} ions next to the molecular adsorbate as well as the alignment of the porphyrin adsorbate along the [101], [010] and [-101] directions . [23] The IET software was obtained from Batista group and performed it with considering reported conditions in literature. [22] In summary, we have computed the survival probability, p(t), defined as the probability that the photoexcited electron remains in the adsorbate molecule at different times (t) after excitation of the system. Computing the time-dependent wave function $|\Psi(t)\rangle = \sum_i Bi(t)|\chi i\rangle$, expanded in the basis set of AOs $|\chi i\rangle$, required the propagation of the expansion coefficients Bi(t)) $\sum_q Q_i{}^q C_q \exp[-(i/\hbar)E_q t]$, where C_q is the expansion coefficient of the initial state $|\Psi(0)\rangle = \sum_q C_q|q\rangle$. To avoid artificial recurrences in electron-transient populations, the calculations of charge injection were conducted in models consisting of a 3×3 adsorbate-anatase super cell array. Initial states are defined in terms of the excited electronic states of the adsorbate with significant electronic couplings with the semiconductor conduction band [24].

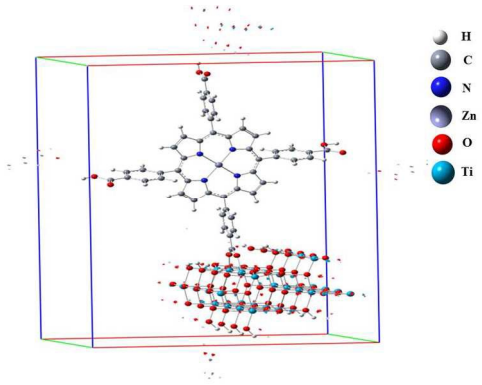

Figure 1. Nanostructure of TiO_2-anatase sensitized by Zn TCPP after geometry relaxation under vacuum conditions and electronic density in the highest occupied molecular orbital.

2.3 . Synthesis of porphyrin dyes. 2.1 H_2TCPP [25, 26] (300 mg, 0.38) and zinc(II) acetate (166 mg, 0.75mmol) were dissolved in DMF (80 mL), and the solution was stirred at reflux for 45 min. The metal complex formation was monitored by UV-Vis spectroscopy in DMF. After filtration, DMF were evaporated under vacuum and the residue was washed with water to remove the excess metal salt. UV-Vis (DMF): λ_{max}(nm): 423, 556, 598.

2. 2. Bromination of ZnTCPP ($ZnTCPPBr_x$) (X = 2 and 8)

Dibromo-meso-tetrakis-(4-phenyl carboxyl) porphyrinato Zinc(II)complex ($ZnTCPPBr_2$). $ZnTPPBr_2$ was prepared according to the literature. [27] ZnTCPP (200 mg, 0.23 mmol) was dissolved in THF (40 ml). To this solution, freshly recrystallised NBS (166 mg, 0.93 mmol) was added. The reaction mixture was stirred for 24 h at room temperature and then the solution was evaporated to dryness. The solid was then dissolved in chloroform and washed several times with distilled water in a separating funnel.

Octabromo-meso-tetrakis-(4-phenyl carboxyl) porphyrinato Zinc(II) complex ($ZnTCPPBr_8$). $ZnTCPPBr_8$ was prepared starting from ZnTCPP (150 mg, 0.175 mmol) and freshly recrystallised NBS (0.779 g, 4.489 mmol) using the same procedure as described for $ZnTCPPBr_8$ to yield the product.

The degree of bromination of ZnTCPP and the purity of $ZnTCPPBr_x$ have been determined by ^{1}H NMR spectrometry based on the ratio of the intensities of the signals corresponding to the protons from H_β and meso substituents (H_β/H_{ortho} and H_β/H_{meta} ratios); in the case of $ZnTCPPBr_2$, a value of ca. 0.75 was observed for both the H_β/H_{ortho} and H_β/H_{meta} ratios. In the case of $ZnTPPBr_8$ the signal due to the β protons disappeared. Also,

ICP analysis was used to confirm the elemental composition of the brominated zinc porphyrins.

2. 4. Fabrication of DSSC. TiO_2 photoelectrode was prepared by screen-printing methods. TiO_2 photoelectrode (area: ca. 0.3 cm × 1cm) was prepared by a similar method reported in the literature. [28] Nanocrystalline TiO_2 films of 10–15 μm thickness were deposit ed onto transparent conducting glass (which has been coated with a fluorine-doped stannic oxide layer, thickness of 5 mm, sheet res istance of 20–25X). These films were dried at 150 ˚C for 30 min and then were gradually sintered at 450 ˚C for 30 min. The sensiti zer was dissolved in ethanol at a concentration of 1×10^{-4} mol L^{-1}. The photoelectrode was dipped into the dye solution immediately kept at room temperature for 24 h so that the dye was adsorbed o nto the TiO_2 films. A sandwich cell was assembled by using the d ye anchored TiO_2 films as the working electrode and conducting glass coated with Pt as the counter electrode. The two electrodes were placed on top of each other. The electrolyte was introduced i nto cell through a syringe between two electrodes. The compositi on of electrolyte was 0.05 mol L^{-1} iodine, 0.1 mol L^{-1} LiI and 0.5 molL^{-1} 4-tert-butylpyridinein acetonitrile. Photoelectrochemical d ata were obtained using a 450 W Xenon light source focused to gi ve 100 mW cm^{-2}, the equivalent of one sun at AM 1.5 at the surfa ce of the test cell.

3. Results and discussion

3.1 Absorption spectroscopy.

The molecular structures of H_2TCPP (1), $ZnTCPPBr_2$ (2) and Zn $TCPPBr_8$ (3) are shown in Scheme 1.

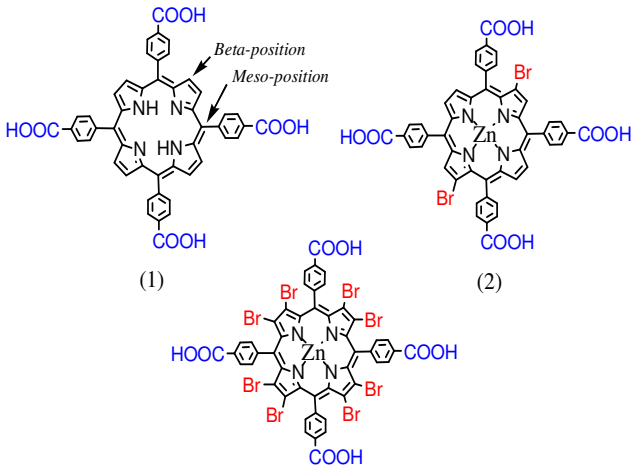

Scheme 1. Molecular structures of (1), $ZnTCPPBr_2$ (2) and ZnTC $PPBr_8$ (3).

The strong absorption of porphyrins in the 400-450 nm region (S oret band) as well as absorptions in the 500-700 nm region (Q-ba nds) [5] make them excellent candidates as photosensitizers in solar cells. The UV–Vis absorption spectra of ZnTCPP, $ZnTCPPBr_2$ an d $ZnTCPPBr_8$ in THF are shown in Fig. 2. Also, the peak positions of the Soret and Q bands of porphyrin dyes are summarized in Table 1.

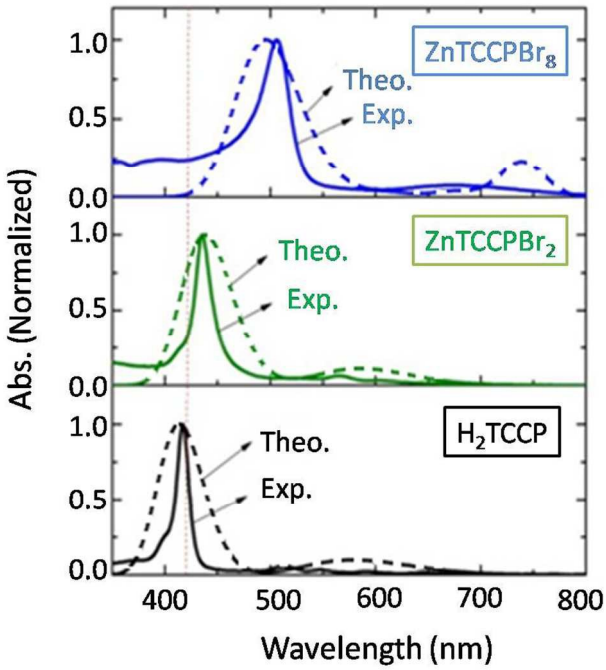

Figure 2. Absorption spectra of H_2TCPP, $ZnTCPPBr_x$(X= 2 and 8) in THF solution 10^{-5} mol lit^{-1} (solid lines). Computed UV-Vis s pectra of dyes are also shown, obtained at the TD-DFT/(LanL2D Z) level of theory (dashed lines).

As seen in Figure 2, there is a systematic red shift in λ_{max} of Soret band upon increasing the number of Br groups at the β positions. The UV–Vis absorption spectrum of H_2TCPP exhibits a strong S oret band at 417 nm and four weak Q-bands at 513, 548, 591 and 648 nm. On the other hand, the Soret and Q bands of $ZnTCPPBr_2$ appear at 435, 566 and 606 nm, respectively which are red-shifted with respect to those of H_2TCPP, However, $ZnTCPPBr_8$ showed a strong absorption band at 506 nm and a broad one at 675 nm, w hich are broader and more red-shifted compared to those of the ot her compounds. As seen in the UV–Vis absorption spectra, the So ret band of $ZnTCPPBr_2$ and $ZnTCPPBr_8$ are red-shifted about 18 and 89 nm compared to that of H_2TCPP, respectively.

Table 1. Experimental and theoretical UV-Vis data for H_2TCPP, $ZnTCPPBr_x$ x=2 and 8.

Compounds	Soret band (nm)	Q_{IV} band (nm)	Q_{III}	Q_{II}	Q_I
H_2TCPP_{Exp}	417	513	548	591	648
$H_2TCPP_{Theo.}$	408		-	564	-
$ZnTCPPBr_{2Exp}$	435	565	-	606	-
$ZnTCPPBr_{2Theo.}$	437	553	-	-	-
$ZnTCPPBr_{8Exp}$	506	-	-	675	-
$ZnTCPPBr_{8Theo.}$	495	-	-	740	-

The simulated absorption spectra for H_2TCPP, $ZnTCPPBr_x$ (X=2 and 8), obtained by the TD-DFT calculation, are also shown in Fi gure 2. The shape and the main peaks of the spectra reproduce the experimental data reasonably well.

Hence, we can quantitatively probe the porphyrin geometry by m easuring wavelengths of each $ZnTCPPBr_x$ derivative as a function of the number of Br groups on the macrocycle. [29, 30] As shown in Figure 2, the theoretical results suggest that the Soret and visible

absorption bands of the porphyrins are highly sensitive to peripheral substitution. Similar spectral trends were also observed for different isomers of $ZnTPPBr_x$ which was suggested that the red shift in absorption bands of the brominated porphyrins can be attributed to both an electron-withdrawing effect of the Br groups and a nonplanarity of the macrocycle caused by steric factors. [31] However, significant red shifts in the UV-Visible spectra often serve as a signature of porphyrins non-planarity. [32] Nonplanar distortions includes Ruffle, Saddle, Dome and Wave distortions are well-established for both synthetic porphyrins as well as for biological applications [33, 34] (Figure 3).

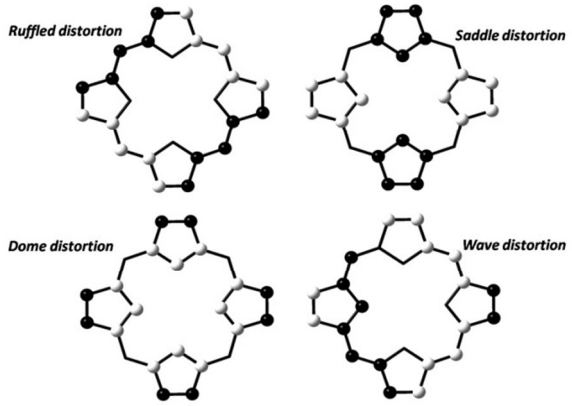

Figure 3. Schematic depiction of ruffled, saddled, domed and waved conformations. The black and white circles indicate displacements on opposite sides of the mean plane of the porphyrin.

The saddle conformation caused by Br groups on the nonplanarity of the macrocycle is illustrated in Figure 4.

The presence of a large red shift for peripherally substituted nonplanar porphyrins has also been proved by a number of studies where the electronic effect of the substituents is more carefully controlled for a series of porphyrins.[35]

In addition, X-ray structure determination of the β -pyrrole brominated porphyrins proved the saddle-shaped conformation.[36, 37] In general, porphyrin nonplanarity can cause the changes in the a_{1u} and a_{2u} HOMOs levels and the narrowing of the HOMO–LUMO gap by distorting D_{4h} porphyrins complexes to those of D_2 symmetry as observed for β-substituted TFPP (tetrakis (penta fluorophenyl)porphinato) complexes.[33] This issue will be discussed in following.

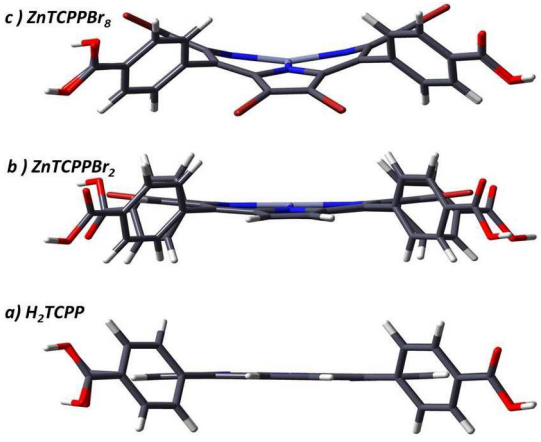

Figure 4. The saddle-shaped $ZnTCPPBr_8$.caused by Br atom substitution.

These results suggest that UV−visible band red-shifts of β-pyrrolic substituted nonplanar porphyrins are potentially useful candidate for the enhancement of light harvesting provided highly efficiency dye sensitized solar cell based on Saddle-shaped porphyrins.

3. 2. DSSC measurements. Investigations into the solar energy conversion to electricity of the β-pyrrolic substituted porphyrins linked to a semiconductor surface are rare. [38] On the basis of evidences which mentioned in pervious section, we expected the increasing of overall conversion efficiency in brominated porphyrins compared to non-brominated porphyrins.

Thus, DSSCs were fabricated using H_2TCPP, $ZnTCPPBr_x$(X= 2 and 8) as the sensitizers, with an effective area of 0.4 cm^2, single-layer TiO_2 film with 10–15 μm thickness on FTO, and the electrolyte composed of 0.1 M LiI, 0.05 M I_2, and 0.5 M 4-tert-butyl-pyridine (TBP) in acetonitrile solvent. The photovoltaic performance of the Zn-porphyrin-sensitized TiO_2cells was obtained. Figure 5 shows the J–V curve of DSSCs based on $ZnTCPPBr_8$.

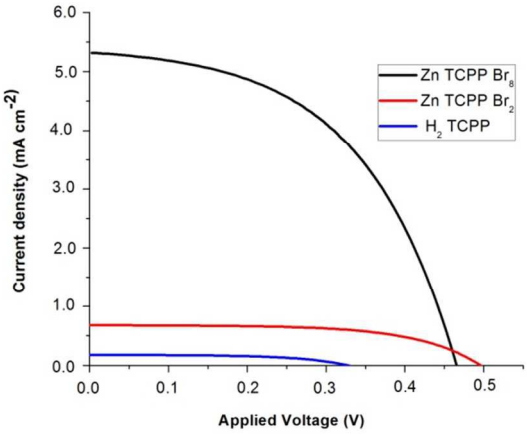

Figure 5. J–V curve of DSSCs sensitized with H_2TCPP, $ZnTCPPBr_2$, $ZnTCPPBr_8$.

The detailed parameters (J_{sc}, V_{oc}, ff, and η) are summarized in Table 2. The DSSCs based on brominated Zn-porphyin dyes shows a better comprehensive properties than DSSC based on H_2TCPP dye under AM 1.5 irradiation (100 mW cm^{-2}).

Table 2: Photovoltaic performances of DSSCs sensitized with H_2 TCPP and $ZnTCPPBr_x$ (x=2 and 8).

Dye	J_{sc} ($mA.cm^{-2}$)	V_{oc} (V)	FF (%)	H (%)	IPCE (%)
H_2TCPP	0.2	0.32	41	0.04	7.3
$ZnTCPPBr_2$	0.7	0.50	57	0.22	14.1
$ZnTCPPBr_8$	5.4	0.46	47	1.17	26.7

In accordance with UV-Vis results, linear relationship is observed between photovoltaic performance of each compound and the number of bromo substituent at the β-pyrrole position of macrocycle. It is easy to see that the V_{oc} of H_2TCPP dye is lower than that of the brominated Zn-porphyrins. To a large extent, the two brominted Zn-porphyrin dyes display higher J_{sc} than H_2TCPP. The different η values of the three porphyrin-sensitized primarily result from the difference of J_{sc}. The biggest difference in J_{sc} values, between the brominated dyes and non- brominated dye is because the efficient injection of electrons into TiO_2 conduction band. This subject will be discussed in following.

Action spectrum, incident photon-to-electron conversion efficiency (IPCE) as a function of wavelength, was measured to evaluate the photoresponse of photoelectrode in the whole spectral region. Figure 6 shows the IPCE spectra of DSCs based on H_2TCPP, $ZnTCPPBr_2$ and $ZnTCPPBr_8$ dyes onto TiO_2 . Three dyes can convert visible light to photocurrent in the range of 400-700 nm. $ZnTCPPBr_8$ anchored TiO_2 gave broader spectra and higher photoresponse in the long wavelength region (>500 nm) than other dyes, which was consistent with the corresponding absorption spectra. IPCE performance clearly indicated that bromine substitution on porphyrin macrocyle makes the red-shift of IPCE spectra. FT-IR spectroscopy has been shown to be a powerful tool for extracting structural information of the molecules adsorbed onto a TiO_2 surface. Figure 7 shows FT-IR spectra of H_2TCPP, $ZnTCPPBr_x$ and their complexes adsorbed onto TiO_2 films. Figure 7 shows spectra of dyes with a strong adsorption at 1702 cm^{-1} attributable to the ν(C=O) stretching mode of the carboxylic acid group. [38]

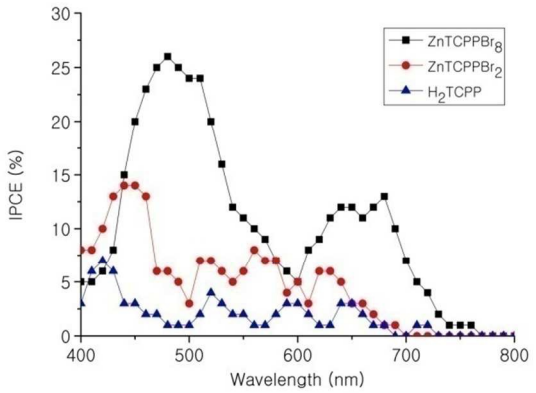

Figure 6. IPCE spectra of nanocrystalline TiO_2 films sensitized by H_2TCPP, $ZnTCPPBr_x$, X=2 and 8.

The FT-IR spectra of the adsorbed porphyrins onto TiO_2 film do not exhibit typical carboxylic acid vibrational modes, but they all show the presence of carboxylate asymmetric ν ($-COO^-_{as}$) and symmetric ν ($-COO^-_s$) bands at ; for $ZnTCPPBr_2$,these occur about 1625 and 1417 cm^{-1}, respectively. This indicates binding of the porphyrins to the TiO_2 rather than aggregation of the porphyrins on the surface. The difference between $\nu_{as}(COO^-)$ and $\nu_s(COO^-)$ (Δν), compared to the corresponding values in ionic (218cm^{-1}), is currently to determine the corresponding mode of the carboxylte group .[40] The possible binding modes for porphyrins containing carboxylic acid groups on a TiO_2 surface are shown in Figure 8.

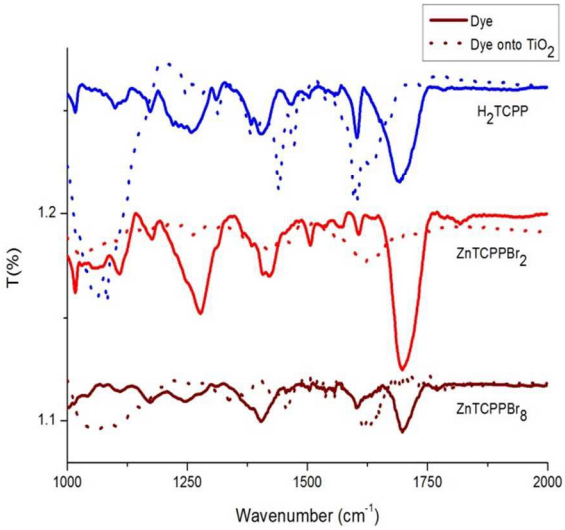

Figure 7. FT-IR spectra of H_2TCPP, $ZnTCPPBr_2$ and $ZnTCPPBr_8$ (solid line) and complexes adsorbed on TiO_2 films (dashed line).

1. The unidentate coordination of the carboxylato group removes the equivalence of the two oxygen atoms, resulting in an ester type of bond formation between the carboxylato group and the TiO_2 surface. Unidentate complexes (figure 8(I)) exhibit the Δν values [$\nu_{as}(COO^-) - \nu_S(COO^-)$] which are much greater than the ionic complexes.
2. Chelating complexes (figure 8(II)) exhibit Δν values which are significantly less than the ionic values.
3. The Δν values for bridging complexes (figure 8(III)) are greater than those of chelating complexes, and close to the ionic values.

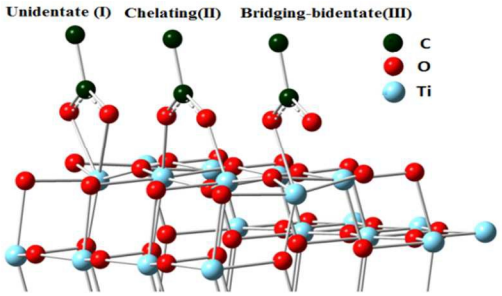

Figure 8. Possible coordination modes for carboxylate anions in the TiO_2 solid state.

On the basis of the FT-IR measurements, the difference between these bands in the ionic value (=218 cm^{-1}) and the adsorbed porphyrins (=208 cm^{-1}), together with other evidence that suggests that the carboxylate groups are bound to the TiO_2 surface via a bridging bidentate mode (III).

3. 3. DFT and TD-DFT calculations. Initial calculations were performed on the synthesized porphyrins to determine the HOMO and LUMO levels of the Zn-porphyrins independently. After the initial calculations, the HOMO and LUMO levels were calculated and compared. These have known cell efficiencies of 0.04, 0.22 and 1.41 for (H_2TCPP), ($ZnTCPPBr_2$), ($ZnTCPPBr_8$), respectively (See Table. 3). Figure 9 shows the four highest and four lowest m

olecular orbital energy levels of the synthesized Zn-porphyrins. It is noteworthy that the HOMO and LUMO energy levels of the br ominated Zn-porphyrins are relatively lower than those of the non -brominated porphyrin. However, higher stabilization of the LU MO levels relative to the HOMO ones makes the HOMO–LUMO gaps of the brominated Zn-porphyrins models smaller compared t o that of the nonbrominated counterparts. This observation seems to be a good explanation for the enhancement of solar cell efficie ncy of the brominated Zn-porphyrins compared to the nonbromin ated ones, as was evident by the experimental results. For the acc eptor moieties, carboxylic acid is the main functional group, and i t is a good anchoring functional group for titanium dioxide. [41]

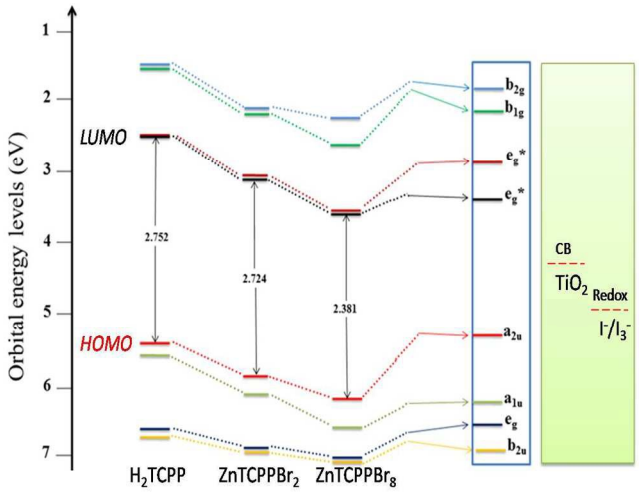

Figure 9. Energy Level Diagrams of H_2TCPP, $ZnTCPPBr_x$ (x=2 a nd 8),TiO_2 and I^-/I_3^-.

The relative positions of the LUMO levels for the donor and acce ptor moieties are very important for charge transport to be effecti ve .[42] The acceptor moieties cited above have a LUMO acceptor d ifference that ranges from approximately 0.21 to 0.75 eV, which i s sufficient for charge transport. Figure 10 shows the HOMO and LUMO orbital spatial orientation of the brominated Zn-porphyrin s and non-brominated porphyrin. Mizusekiet al.[43] suggested tha t the charge transport was related to the spatial distribution of the frontier orbitals. The HOMO should be localized in the donor mo iety and the LUMO in the acceptor moiety .[38] In our calculations, in all porphyrin complexes their HOMO localized in the α and β positions of macrocycle ring region and their HOMO-1 localized in the pyrrolic ring nitrogens and meso-positions that adapted to f rontier molecular orbitals (FMOs) of Gouterman's four-orbital m odel. $ZnTCPPBr_8$ complex have eight bromine groups in their str ucture, which caused the more localization of the LUMO on the a cceptor groups. The presence of zinc metal might be responsible f or the delocalization of both the HOMO and LUMO, suggesting t he presence of a metal-to-ligand charge transfer (MLCT) or metal -centered transitions from both the metal and the ligand π-orbitals in the LUMO.[44] The electron-withdrawing substituents seem to lo calize the HOMO on their sides. The charge-separated state is on e of the main factors affecting solar cell efficiency. Based on our DFT calculations, brominated Zn-porphyrins generally have smal ler HOMO–LUMO gaps than their nonbrominated counterparts. These results may provide structural guidelines for selecting the i dentify candidate porphyrin complexes to be used for higher-level calculations, which could provide actual electronic and structural information about the interface between the dye molecule and se miconductor. The result could also help as a qualitative selection process to synthesize porphyrins for developing an efficient DSS C .

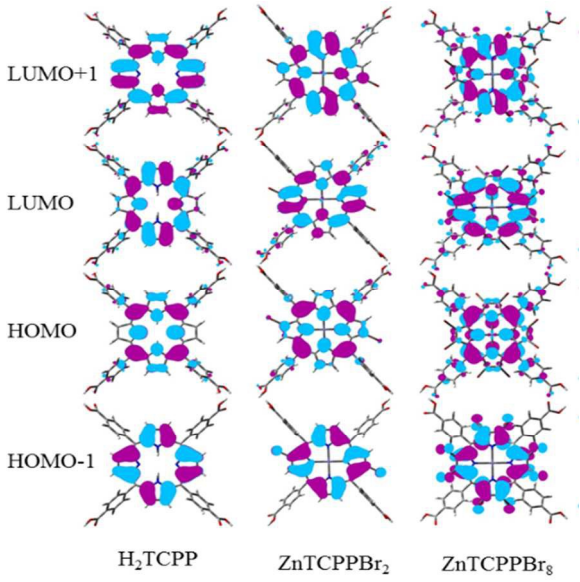

Figure 10. Molecular orbital spatial orientation for H_2TCPP, Z $nTCPPBr_x$ x=2 and 8.

As well as performed TD-DFT calculation in THF solution for th ese porphyrins. According to the Figure 2, there are two main tra nsitions for the $ZnTCPPBr_2$ complex, in wavelengths 437 and 560 nm with *f* 1.71 and 0.07 respectively. In λ= 430 nm, electron trans fer from HOMO-1 (a_{2u}) to LUMO (e_g*), which having percentage %38. When occur the electron transition from HOMO to LUMO, appear Q band at 553 nm in UV/Vis spectrum.

Finally, there are two absorption bands at 495 and 740 nm for Zn $TCPPBr_8$ complex. In wavelength of 495 nm, electron transfer oc curred from HOMO-1 (a_{1u}) to LUMO+1 (e_g*). In continuing, at λ = 740 nm, electrons transferred from HOMO-1 to LUMO with pe rcentage % 49.1 that leads to appearance of the Q band. Accordin g to these calculations, through introduction any bromine atom on β-positions red-shifted Soret band about 5 nm.[9, 38, 45, 46] H. J. Carll ot et al. reported the first observation of a red shift of the Soret ba nd upon β-pyrrole bromination. [47] The decreased HOMO-LUMO gap and the multitude of configuration interactions caused by the introduction of substituent at the periphery of the porphyrin ring h ave been suggested to explain the observed red shifts. [29, 30 , 48-50]

3. 4. Interfacial Electron Transfer simulation.

In focusing on photoinjection mechanisms from the excited electronic states of porphyrin, herein, improvement in the electron injection process to TiO_2 induced by the substitution of bromine atoms at the beta positions of H_2TCPP and the likely application to the design of an efficient $ZnTCPPBr_x$-sensitized solar cell are examined. The Soret and Q bands of porphyrins are associated with an electronic displacement towards the periphery of the aromatic macrocycle. [51] Accordingly, in the excited states of porphyrins, the meso substituents may be considered as the donor part of the macrocycle. Also, upon the coordination of H_2TCPP and $ZnTCPPBr_x$ to the surface of TiO_2, the Ti(IV) centre acts as the acceptor part, due to the Lewis acid strength of the

cation. It should be noted that the oxygen atoms of the –COOH groups, can form strong bonds with the Ti(IV) atom. [52]

Surface sensitization involves the adsorption of a porphyrin to TiO_2 surface and the formation of a porphyrin-TiO_2 surface complex. [24] Photoexcitation of the surface complex will lead to interfacial electron transfer when there is appropriate energy match between the photoexcited electronic state in the surface complex and the electronic states in the conduction band of the TiO_2 semiconductor. Injection times as short as a few femtoseconds have been investigated for various systems whereas charge recombination in the micro to millisecond time scale. [22, 53-55] This result is a sign of the nuclear motion cannot be the rate-determining factor in the underlying IET mechanisms. Therefore, the results of simulations of IET allow us to predict the net rates and probabilities of IET into TiO_2 semiconductor. To investigate the interaction between the sensitizer LUMO orbital and the substrate conduction band, we have made a detailed investigation of the adsorbate LUMO DOS. The density of states (DOS) obtained by the extended Huckel (eH) method for all porphyrin adsorbed on TiO_2 is presented in Figure 11.

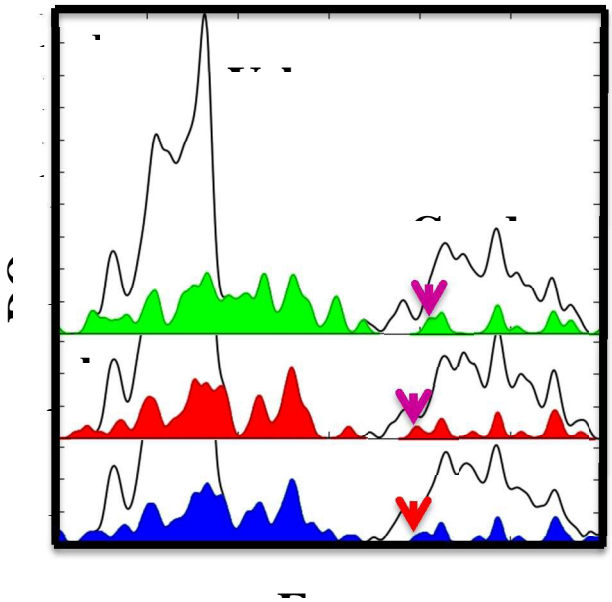

Figure 11. Density of states (DOS) calculated by the extended Huckel theory for functionalized TiO_2 anatase nanostructures with H_2TCPP (a), $ZnTCPPBr_2$ (b) and $ZnTCPPBr_8$ (c) adsorbed to the (101) surface of TiO_2 and a bare TiO_2 anatase nanostructure.

Table 3. The percent of electron injection from adsorbates to TiO_2 anatase crystal at first 25fs after photoexcitation

Time(fs)	0	5	10	15	20	25
H_2TCPP	0%	0.50%	1.85%	0.86%	2.22%	2.49%
$ZnTCPPBr_2$	0%	3.04%	6.17%	4.03%	5.00%	8.75%
$ZnTCPPBr_8$	0%	4.83%	17.32%	35.68%	51.06%	65.69%

Cite this: DOI: 10.1039/c0xx00000x

www.rsc.org/xxxxxx

ARTICLE TYPE

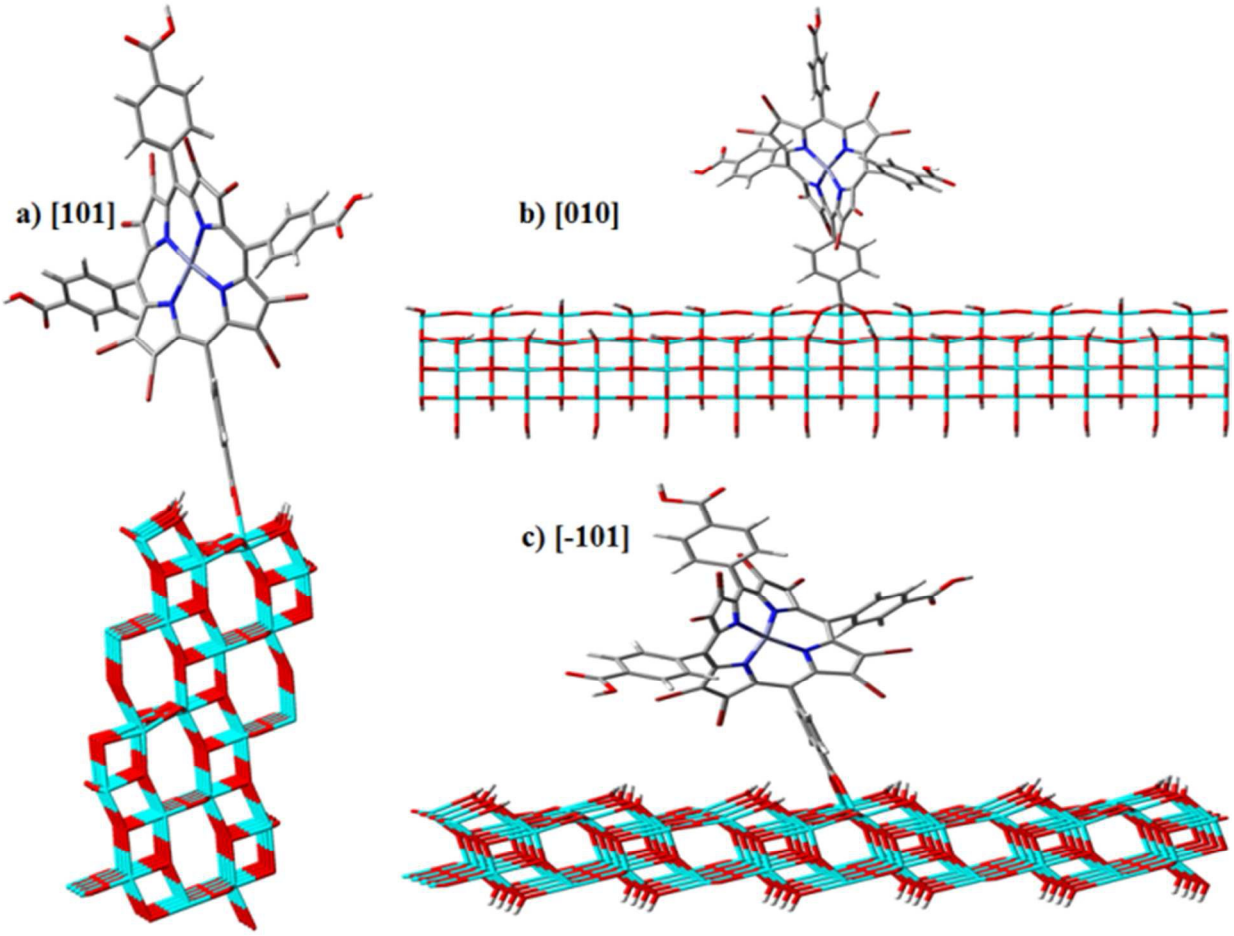

Figure 12.Panels a, b, and c show nanostructures extended along the [101], [010], and [-101] directions in the anatase crystal.

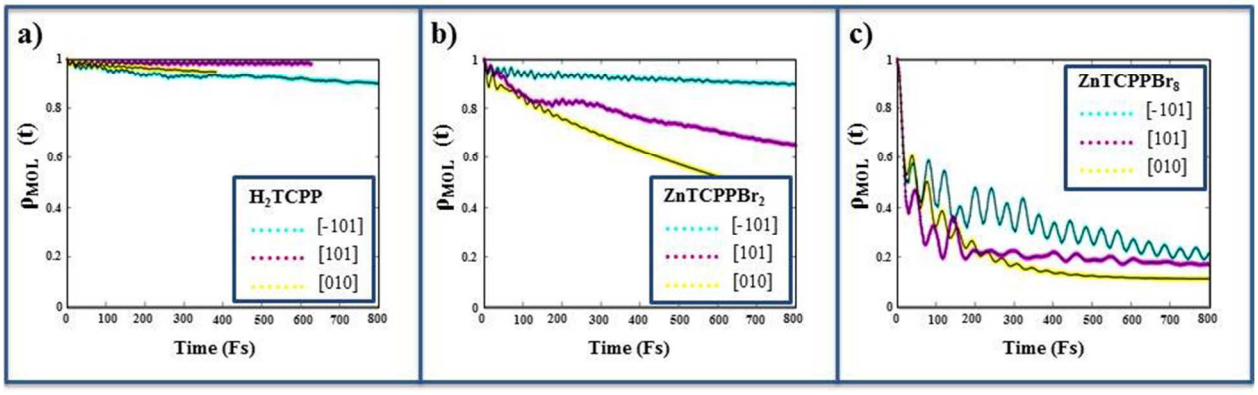

Figure 13. Time-dependent survival probability in sensitized nanostructures extended along the [-101], [010] and [101] crystallographic d irection in the TiO_2 anatase crystal.

The filled solid curve at the bottom of the graph represents the projected density of states on the H_2TCPP, $ZnTCPPBr_2$ and $ZnTCPPBr_8$ basis functions. The DOS plot shows the presence of energy levels from the $ZnTCPPBr_x$-adsorbate in the band gap of TiO_2. Moreover, Figure 11 clearly shows that the investigated systems differ both in the exact position of the LUMO level and the degree to which the sensitizer LUMO orbital mixes with the substrate conduction band. Additionally, there is a number of virtual orbitals (LUMOs) positioned within the conduction band. These orbitals have relatively strong electronic coupling with the conduction band of TiO_2 and can promote efficient IET. [56] To achieve good performance, it has been firmly recognized that the electron injection must be fast and highly efficient and the recombination must be slow. [57-60]

Charge injection occurs from the π*-orbitals of the anchoring group (carboxylic or phosphoric acid) to the titanium 3d-orbitals. A good overlap of these orbitals is mandatory for efficient charge injection. The better overlap between energy levels of LUMO of dye (donor) and the conduction band of TiO_2 (acceptor) is believed to play a crucial role making more favorable the electron injection .[61] In Fig. 6, the energy levels of LUMO of $ZnTCPPBr_2$, $ZnTCPPBr_8$ and the conduction band potential of TiO_2 lies at 3.11, 3.64 and 4.2 eV, respectively . It is clear that electron injection from the excited dyes molecules into the conduction band of the semiconductor is possible, as the driving force for charge displacement into the oxide is about 1.0 eV for the $ZnTCPPBr_2$ dyes, whilst for $ZnTCPPBr_8$ is only 0.46 eV. The excited state of $ZnTCPPBr_8$ dye matches better the lower bound of the conduction band of the semiconductor than the LUMOs of the H_2TCPP and $ZnTCPPBr_2$ dyes, thus minimizing the energetic losses during the electron transfer process. [62] It is important to investigate the convergence properties of the simulation results with respect to the size of the system. This is accomplished by checking convergence in the electron injection times in nanostructures extended along the [-101], [010], and [101] crystallographic directions. [63-65]

Figure 12 shows extended structures generated by replicating nanostructure units along the three [-101], [010], and [101] crystallographic directions.

Smith and Nozik have investigated 1-dimensional and 3-dimensional model systems in an effort to understand the central aspects of interfacial electron transfer as well as the limitations of theoretical approaches such as the Landau-Zener approximation [6] and the Anderson Hamiltonian approach. [22, 66] The distance bond length between the carboxylic groups of formic acid and TiO_2 anatase (101) surfaces represents approximately 2.10, 2.08. [40, 67, 68] As earlier reports on porphyrin adsorbed on TiO_2 surface and FT-IR results, we connect the four dyes under identical conditions to take into account the distance of 2 Å.

Table. 3 shown The percent of electron injection from adsorbates to TiO_2 anatase crystal at first 25 fs after photoexcitation for initial model system. The result as well as shown porphyrin structure substitution of bromine atoms at β pyrrole positions, electron injection is much better and because of the increased efficiency in this category of porphyrins clearly indicates. Figure 13 shows results for the survival probability $\rho_{MOL}(t)$ obtained from simulations of electron injection in nanostructures extended along the[101], [-101] and [010] directions. Exponential fitting curves to $p_{MOL}(t)$ define the approximate characteristic times for the two electron-injection steps in nanostructures extended along the [-101] [010], and [101] direction. The IET rates, >450, ~125, and 25 fs, are observed for the H_2TCPP, $ZnTCPPBr_2$ and $ZnTPPBr_8$, respectively. On the basis of our IET simulations, the excited states of $Zn(TCPPBr_x)$ x=2 and 8 will lead to the electron injection into TiO_2, since they have significant electron population on the phenyl (COOH) ligand attached to the nanoparticle.

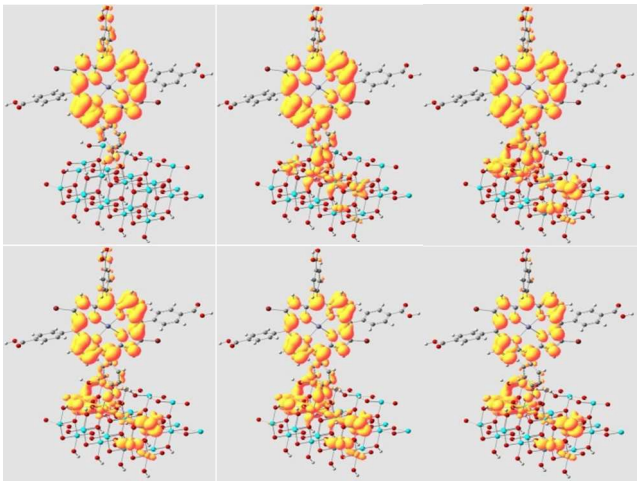

Figure 14. Evolution of time-dependent charge distribution during the early time relaxation dynamics after instantaneously populating the $ZnTCPPBr_2$- LUMO. The individual frames show snapshots of an electronic density isosurface at intervals of 125 fs.

Figure 14 and 15 show a quantitative description of the survival probability as a function of time after instantaneously populating the $Zn(TCPPBr_x)$ (x=2 and 8)-(LUMO) in nanostructures extended along the[-101] directions in the TiO_2-anatase crystal. Note that the frames in Figure 14 describe the electron injection at first 0, 5, 10, 15, 20 and 25 fs. As our calculation results and previous experimental evidences, the electron injection from excited porpyhrin dyes to TiO_2 conduction band usually occurs very rapidly on the femtosecond–picosecond time domain, therefore natural decay of excited porphyrin dyes cannot compete kinetically with charge-transfer processes. According to classical theory of electron transfer developed by Marcus and Hush, the rate of electron transfer , k_{ET} between discrete donor and acceptor levels under non-adiabatic conditions is given by [28, 69]

$$k = \frac{2\pi}{\hbar}\frac{H^2}{\sqrt{4\pi\lambda_r K_r T}} exp\left[\frac{-(\lambda_r + \Delta G_0)}{4\lambda_r K_B T}\right]$$

Where H^2 is the electronic coupling between donor and acceptor state, ΔG_0 the free energy driving force for electron transfer, λ_r the total reorganization energy, T the absolute temperature and $\hbar$ and K_B the radial Planck and Boltzmann constants respectively. The electronic coupling decreases exponentially with increasing distance, d, between the donor and the acceptor as

$$H^2 = H_0^2 \exp(-\beta d)$$

Where β is related to the properties of the medium between donor and acceptor, and H_0^2 is the coupling ate distance d=0 . Therefore, the distance between eg* of porphyrin and conduction band of TiO_2 has an important effect on the rate of electron transfer (k_{ET}) and the shortest distance between eg* of porphyrins and CB of TiO_2 is realized in $ZnTCPPBr_8$. As shown in Table 3, the electron-injection mechanism from $ZnTCPPBr_8$ involves ultrafast interfacial processes where the initial population in the

excited electronic state of the molecular adsorbate decays to about 66% in about first 25 fs. At the same time, the initial population for the excited-state interfacial electron transfer in $ZnTCPPBr_2$ and H_2TCPP decay about 8 % and 2 %, respectively. The analysis of the time-dependent charge distribution also indicates that the population of the $ZnTCPPBr_x$ adsorbate depends on the number of substituted bromine atom, which decays during the different first time scale of dynamics due to a primary electron-injection event. This process concentrates the injected charge in d_{xz} orbitals, next to the surface complex, including the hexa coordinated Ti $^{4+}$ ion and the Ti^{4+} ions that anchor the photoexcited $ZnTCPPBr_x$ adsorbate. [70] The following relaxation mechanism involves charge diffusion and surface-charge separation. Interestingly, the electron injection at first 10 fs is slower than second 10 fs in $ZnTCPPBr_8$ (Table 3). IET results of $ZnTCPPBr_8$ indicate that the time relaxation can be investigated by an ultrafast (τ=25 fs) electron-injection event that involves a population decay in the molecular adsorbate to about 67% during the first 25 fs of dynamics. Therefore, IET simulation is clearly demonstrated that the increasing of charge distribution is one of accounts for higher conversion efficiency in $ZnTCPPBr_8$.

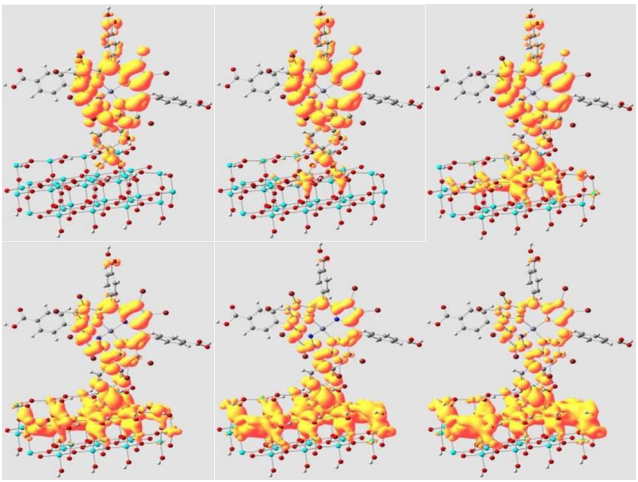

Figure 15. Evolution of time-dependent charge distribution during the early time relaxation dynamics after instantaneously populating the $ZnTCPPBr_8$- LUMO. The individual frames show snapshots of an electronic density isosurface at intervals of 5fs.

We expected that the various fundamental properties elaborated in this study would be beneficial to the future development of halogenated-porphyrin sensitizer for use as DSSCs.

The authors wish to thank the University of Zanjan for financial supports.

4. Conclusion

We have shown that the substitution of bromine atoms at β-pyrrole positions in 5, 10, 15, 20-tetrakis(4-carboxyphenyl) porphyrin zinc(II) complexes has an effect on the photovoltaic performance and life times of the excited electronic states, which, in turn, can influence the electron transfer process between the dyes and the conduction bands of the TiO_2. In addition, the dramatic red-shift in excitation energies observed experimentally and theoretically upon β-bromination of the porphyrin are qualitatively reproduced by the calculations using H_2TCPP, $ZnTCPPBr_2$ and $ZnTCPPBr_8$. The results of DFT and TD-DFT calculations suggest that the changes in the electronic absorption spectra of the fully β brominated porphyrin can be attributed to nonplanarity of the porphyrin macrocycle caused by steric factors. Finally, this view that the large red shifts seen in the UV-visible absorption bands of β-pyrrolic substituted nonplanar porphyrins are the result of saddle-shaped deformations of the porphyrin macrocycle has been employed for enhancement the harvesting in DSSCs.

Although this work does not decide to show an easy rationalization of various parameters, it is clear that, bromo substituents at β-pyrrole positions in porphyrins affect its light harvesting ability in dye sensitized solar cells. This paper opens the way for a more in depth investigation of this new approach.

References

(1) (a) B. O'Regan, M. Gratzel, *Nature.* 1991, **353**, 737-740. (b) M. Urbani, M. Grä tzel, M. Kh. Nazeeruddin, T. Torres, *Chem. Rev*. 2015, doi: 10.1021/cr5001964. (c).T. Higashino, H. Imahor, , *Dalton Trans*., 2015, **44**, 448–463.

(2) L-L. Li , E. W-G.Diau, *Chem. Soc. Rev.*, 2013, **42**, 291-304.

(3) (a) A. Hagfeldt, G. Boschloo, L. Sun, L. Kloo, H. Pettersson, *Chem. Rev*. 2010, **110**, 6595–6663. (b) H. L. Jia, Z. M. Ju, H.X. Sun, X. H. Ju, M. D. Zhang, X. F. Zhou, H. G. Zheng, , *J. Mater. Chem. A*, 2014, **2**, 20841–20848.

(4) (a) H. Imahori, T. Umeyama, S. Ito, *Acc. Chem. Res*. 2009, **42**, 1809–1818. (b) M. J. Griffith,K. Sunahara, P. Wagner, K. Wagner, G. G. Wallace, D. L. Officer, A. Furube, R. Katoh, S. Mori , A. J. Mozer, *Chem. Commun*., 2012, **48**, 4145–4162.

(5) (a) A. Forneli, M. Planells, M. A. Sarmentero, E. Martinez-Ferrero, B. C. O'Regan, P. Ballester, E. Palomares, *J. Mater. Chem*. 2008, **18**, 1652–1658. (b) J. Zhang, J. Z. Zhang, H. B. Li, Y. Wu, Y. Geng , Z. M. Su, *Phys. Chem. Chem. Phys*., 2014, **16**, 24994—25003.

(6) S. Mathew, A. Yella, P. Gao, R. Humphry-Baker, F. E. CurchodBasile, N. Ashari-Astani,I. Tavernelli, U. Rothlisberger, K. NazeeruddinMd and M. Gratzel, *Nat. Chem*., 2014, **6**, 242–247.

(7) (a) R. Kumar, M. Sankar, *Inorg. Chem*. 2014, **53**, 12706–12719. (b) C. Stangel, A. Bagaki, P. A. Angaridis, G. Charalambidis, G. D. Sharma, A. G. Coutsolelos, *Inorg. Chem*. 2014, **53**, 11871–11881. (c) V. Nikolaou, P. A. Angaridis, G. Charalambidis, G. D. Sharma, A. G. Coutsolelos , Dalton Trans. 2015, DOI: 10.1039/c4dt03194f. (b) A. Yella, H. W. Lee, H. N. Tsao, C. Yi, A. K. Chandiran, M. K. Nazeeruddin, E. W. G. Diau, C. Y. Yeh, S. M. Zakeeruddin, M. Gratzel, *Science* 2011, **334**, 629–634.

(8) (a) C. L. Wang, J. Y. Hu, C. H. Wu, H. H. Kuo, Y. C. Chang, Z. J. Lan, H. P. Wu, E. W. G. Diau, C. Y. Lin, *Energy Environ. Sci.,* 2014, **7**, 1392-1396. (b) C. H. Wu, M. C. Chen, P. C. Su, H. H. Kuo, C. L. Wang, C. Y. Lu, C. H. Tsai, C. C. Wu, C. Yao Lin, *J. Mater. Chem. A*, 2014, **2**, 991–999. (c) H. P. Wu, Z. W. Ou, T. Y. Pan, C. M. Lan, W. K. Huang, H. W. Lee, N. M. Reddy, C. T. Chen, W. S. Chao, C. Y. Yeh, E. W. G. Diau, *Energy Environ. Sci.*, 2012, **5**, 9843-9848. (d) J. Luo, M. Xu, R. Li, K. W. Huang, C. Jiang, Q. Qi, W. Zeng, J. Zhang, C. Chi, P. Wang, J. Wu, *J. Am. Chem. Soc.*, 2014, **136**, 265–272. (e) C. Jiao, N. Zu, K. W. Huang, P. Wang, J. Wu, *Org. Lett.*, 2011, **13**, 3652–3655.

(9)(a) J. W. Penny, C. G. Keith, L. O. David, M. C. Wayne, *J. Mole. Struct: Theochem*. 2006, **759**, 17–24. (b) K. B. Ørnsø, C. S. Pedersen, J. M. Garcia-Lastra, K. S. Thygesen, *Phys. Chem. Chem. Phys.*, 2014, **16**, 16246—16254.

(10) S. Cherian, C. C. Wamser, *J. Phys. Chem. B*. 2000, **104**, 3624-3629.

(11) P. Ochsenbein, K. Ayougou, D. Mandon, J. Fischer, R. Weis

s, R. N. Austin, K. Jayaraj, A. Gold, J. Terner, F. Fajer, *Angew. C hem. Int. Ed. Eng*. 1994, **33**, 348-350.
(12) M. S. Le Cours, G. S. DiMagno, J. M. Therien, *J. Am. Chem. Soc.* 1996, **118**, 11854–11864.
(13) P. J. Spellane, M. Gouterman, A. Antipas, S. Kim, Y. C. Liu, *Inorg. Chem*. 1980, **19**, 386-391.
(14) M. Gouterman, Spectra of porphyrins, *J. Mole. Spec*., 1961, **6**, 138-163.
(15) F. D'Souza, K. Kadish, Electron Transfer Processes of β-Pyrrole Brominated Porphyrins: Structural vs. Electronic Effects. *N4-Macrocyclic Metal Complexes N4-Macrocyclic Metal Complexes*. 2006, pp-439-466.
(16) F. D'Souza, E. M. Zandler, P. Tagliatesta, Z. Ou, J.Shao, V. E. Caemelbecke, M. K. Kadish, *Inorg. Chem*. 1998, **37**, 4567-4572.
(17) D. Mandon, P. Ochsenbein, J. Fischer, R. Weiss, K. Jayaraj, N. R. Austin, S. P. White, O. Battioni, *Inorg. Chem*. 1992, **3**, 2044-2049.
(18) H. He, Y. Zhong, L. Si, A. Sykes, *Inorg. Chim. Acta*, 2011, **378**, 30-35.
(19) K. Ladomenou, T. N. Kitsopoulos, G. D. Sharma, A. G. Coutsolelos, *RSC Adv*., 2014, **4**, 21379–21404.
(20) E. Jakubikova, C. R. Snoeberger III, V. S. Batista, L. R. Martin, R. E.Batista, *J. Phys. Chem. A*, 2009, **113**, 12532–12540.
(21) M. J. Frisch, G. W. Trucks, H. B. Schlegel, , G. E. Scuseria, M. A. Robb, J. R.Cheeseman, J. A. Montgomery, T. Vreven, K. N. Kudin, J. C. Burant, J. M. Millam, S. S. Iyengar, J. Tomasi, V. Barone, B. Mennucci, M. Cossi, G. Scalmani, N. Rega, , G. A. Petersson, H. Nakatsuji, M. Hada, M. Ehara, K. Toyota, R. Fukuda, J. Hasegawa, M. Ishida, T. Nakajima, Y. Honda, O. Kitao, H. Nakai, M. Klene, X. Li, J. E. Knox, H. P. Hratchian, J. B. Cross, V. Bakken, C. Adamo, J. Jaramillo, R. Gomperts, R. E. Stratmann, O. Yazyev, A. J. Austin, R. Cammi, C. Pomelli, J. W. Ochterski, P. Y. Ayala, K. Morokuma, G. A. Voth, P. Salvador, J. J. Dannen-berg, V. G. Zakrzewski, S. Dapprich, A. D. Daniels, M. C. Strain, O. Farkas, D. K. Malick, A. D. Rabuck, K. Raghavachari, J. B. Foresman, J. V. Ortiz, Q. Cui, A. G. Baboul, S. Clifford, J. Cioslowski, B. B. Stefanov, G. Liu, A. Liashenko, P. Piskorz, I. Komaromi, R. L. Martin, D. J. Fox, T. Keith, M. A. Al-Laham, C. Y. Peng, A. Nanayakkara, M. Challacombe, P. M. W. Gill, B. Johnson, W. Chen, M. W. Wong, C. Gonzalez, J. A.,Pople, Gaussian 03 Revision B.04, Gaussian Inc., Wallingford, *CT*, **2004**.
(22) G. C. L. Rego, V. S. Batista, *J. Am. Chem. Soc*. 2003, **125**, 7989-7997.
(23) J. K. Burdett, T. Hughbanks, G. J. Miller, J. W.Richardson, J. V. Smith, *J. Am. Chem. Soc*. 1987, **109**, 3639-3646.
(24) W. R. McNamara, R. C. Snoeberger III, G. Li, J. M. Schleicher, C. W. Cady, M. Poyatos, C. A. Schmuttenmaer, R. H. Crabtree, G. W. Brudvig, V. S. Batista, *J. Am. Chem. Soc*. 2008, **130** , 14329–14338.
(25) D. A. Adler, R. F. Longo, J. A. Finarelli, *J. Org. Chem.* 1979, **32**, 476-476.
(26) D. A. Adler, R. F. Longo, W. Shergalis, *J. Am. Chem. Soc.* 1964, **86**, 3145-3149.
(27) P. Tagliatesta, J. Li, M. Autret, E. Van Caemelbecke, A. Villard, F. D'Souza, K. M. Kadish, *Inorg. Chem*. 1996, **35**, 5570-5576.
(28) (a) M. K. Nazeeruddin, A. Kay, 1. Rodicio, R. Humpbry-Baker, E. Miiller, P. Liska, N. Vlachopoulos, M. Gratzel, *J. Am. Chem. Soc*. 1993, **115**, 6382-6390. (b) H. Shahroosvand, F. Nasouti , A. Sousaraei , *Dalton Trans.*, 2014, **43**, 5158-5167.
(29) P. Bhyrappa, B. Purushothaman, B. *Chem. Phys. Lett*. 2001, **342**, 39–44.
(30) P. Bhyrappa, B. Purushothaman, J. Vittal, *J. Porphyrins Phthalocyanines*. 2003, **7**, 682–692.
(31) H. Ryeng, A. Ghosh, *J. Am. Chem. Soc*. 2002, **124**, 8099-8103.
(32) A. B. J. Parusel, T. Wondimagegn, A. Ghosh, *J. Am. Chem. Soc*. 2000, **122**, 6371-6374.
(33) A. Harad, Y. Matsuda, H. Okawa, R. Miyamoto, S. Yamauchi, T. Kojima, *Inorg. Chim. Acta*. 2005, **358**, 2489–2500.
(34) J. A. Shelnutt, X. Song, J. Ma, S. Jia, W. Jentzen, C. J. Medforth, *Chem. Soc. Rev.*, 1998, **27**, 31-41.
(35) R. E. Haddad, S. Gazeau, J. Pécaut, J. Marchon, C. J. Medforth, J. A. Shelnutt, *J. Am. Chem. Soc*. 2003, **125**, 1253-1268.
(36) H. Duval, V. Bulach, J. Fischer, M. W. Renner, J. Fajer, R. Weiss, *J. Biol. Inorg. Chem.* 1997, **2**, 662–666.
(37) O. S. Senge, G. Vanessa, K. Ruhlandt-Senge, S. Runge, I. Leman, *J. Chem. Soc., Dalton Trans*. 1998, 4187–4199.
(38) W. M. Campbell, A. K. Burrell, D. A. Officer, K. W. Jolley, *Coord. Chem. Rev*. 2004, **248**, 1363–1379.
(39) (a) K. Nakamato, Infrared and Raman Spectra of Inorganic and Coordination Compounds Part II: Application in Coordination, Organometallic and Bioinorganic, John Wiley & Sons , NewYork , NY, USA, 1997. (b) J. Roales, J. M. Pedrosa, P. Castillero, M. Cano, T. M. Richardson, A. Barranco, A. R. González-Elipe, *ACS Appl. Mater. Interfaces*. 2012, **4**, 5147–5154.
(40) Md. K. Nazeeruddin, R. Humphry-Baker, D. L. Officer, W. M. Campbell, A. K. Burrell, M. Gratzel, *Langmuir*, 2004, **20**, 6514-6517.
(41) F. Odobel, E. Blart, M. Lagree, M. Villieras, H. Boujtita, N. El. Murr, S. Caramori, C. A. Bignozzi, *J. Mater. Chem*. 2003, **13**, 502-510.
(42) M. Al-Ibrahim, A. Konkin, H. K. Roth, D. Egbe, E. Klemm, U. Zhokhavets, G. Gobsch, S. Sensfuss, *Thin Solid Films*. 2005, **474**, 201-210.
(43) H. Mizuseki, K. Nimura, C. Majumder, R. V. Belosludov, A. A. Farajian, Y. Kwazoe, *Mol. Cryst. Liq. Cryst*. 2003, **406**, 205-211.
(44) J. P. Sauvage, J. P. Collin, J. C. Chambron, S. Guillerez, C. Coudret, V. Balzani, F. Barigelletti, L. De Cola, L. Flamigni, *Chem. Rev*. 1994, **94**, 993-1019.
(45) A. B. F. Martinson, T. W. Hamann, M. J. Pellin, J. T. Hupp, *Chem. Eur. J*. 2008, **14**, 4458–4467.
(46) K. M. Kadish, F. D'Souza, A. Villard, M. Autret, E. Van Caemelbecke, P. Bianco, A. Antonini, P. Tagliatesta, *Inorg. Chem*. 1994, **33**, 5169-5170.
(47) H. J. Carllot, *Bull. Soc. Chim. Fr.* 1974, **8**, 1492-1496.
(48) S. Rayati, S. Zakavi, S. H. Motlagh, V. Noroozi, M. Razmjoo, A. Wojtczak, A. Kozakiewicz, *Polyhedron*, 2008, **27**, 2285-2290.
(49) W. Jentzen, M. C. Simpson, J. D. Hobbs, X. Song, T. Ema, N. Y. Nelson, C. J. Medforth, K. M. Smith, M. Veyrat, *J. Am. Chem. Soc*. 1995, **117**, 11085-11097.
(50) J. A. Hodge, M. G. Hill, H. B. Gray, *Inorg. Chem*. 1995, **34**, 809-812.
(51) (a) S. F. Mason, *J. Chem. Soc*., 1958, 976. (b) W. J. Weigl, *J. Mol. Spectry*., 1957, **1**, 133. (c) J. R. Platt, *Radiation Biology,* edited by A. Hollaender , McGraw-Hill Book Company, Inc., New York, 1956, Vol. III, ch. 2.
(52)Q. Qu, H. Geng , R. Peng , Q.Cui , X. Gu , F. Li , M. Wang, *Langmuir*, 2010, **26** , 9539–9546.
(53) S. G. Abuabara, L. G. C. Rego, V. S. Batista, *J. Am. Chem. Soc*. 2005, **127**, 18234–18242.
(54) L. G. C. Rego, S. G. Abuabara, V. S. Batista, *J. Chem. Phys.* 2005, **122**, 154709-154714.

(55) L. G. C. Rego, S. G. Abuabara, V. S. Batista, *J. Mod. Opt*. 2006, **53**, 2519–2532.
(56) P. Persson, M. J. Lundqvist, R. Ernstorfer, W. A. Goddard, F. Willig, *J. Chem. Theory Comput*. 2006, **2**, 441-451.
(57) S. A. Haque, E. Palomares, B. M. Cho, A. N. M. Green, N. Hirata, D. R. Klug, J. R. Durrant, *J. Am. Chem. Soc*. 2005, **127**, 3456–3462.
(58) R. Sánchez-de-Armas, J. Oviedo, M. S. Miguel, J. Sanz, *J. Phys. Chem. C*. 2011, **115**, 11293-11301.
(59) K. Ryuzi, F. Akihiro, V. B Alexander, A. Hironori, T. Masanori, *Coord. Chem. Rev*. 2004, **248**, 1195-1213.
.(60) M. G. Griffith, K. Sunahara, P. Wagner, K. Wagner, G. Wallace, D. L. Officer, A. Furube, R. Katoh, S. Mori, A. J. Mozer, *Chem. Commun*. 2012, **48**, 4145–4162.
(61) K. Srikanth, V. R. Marathe, M. K. Mishra, *Int. J. Quantum Chem*. 2002, **89**, 535-549.
(62) T. Stergiopoulos , S. Karakostas , P. Falaras, *J. Photochem. Photobiol. A: Chem*. 2004, **163**, 331-340.
(63) S. Das, C. D. Incarvito, R. H. Crabtree, G. W. Brudvig, *Scie nce.* 2006, **312**, 1941-1943.
(64) R. Rodríguez, M. A. Blesa, A. E. Regazzoni, *J. Colloid Inte rface Sci*. 1996, **177**, 122-131.
(65) C. O'Rourke, C. A. Bowler, *J. Phys. Chem. C.* 2010, **114**, 20 240–20248.
(66) B. B. Smith, A. A. Nozik, *J. Phys. Chem. B*. 1999, **103**, 9915 -9932.
(67) A. Foster, R. M. Nieminen, *J. Chem. Phys.* 2004, **121**, 9039-9042.
(68) M. Nilsing, P. Persson, L. Ojamae, *Chem. Phys. Let.* 2005, **4 15**, 375–380.
(69) (a) R. A. Marcus, *J. Phys. Chem.*, 1956, **24**, 966-978. (b) R. A. Marcus, *Ann. Rev. Phys. Chem*., 1964, **15**, 155-196. (c) N. S. Hush, *J. Chem. Phys*., 1958. **28**, 962-976. (d) N. Hush, *Prog. Inorg. Chem*., 1967, **8**, 391-444.
(70) S. G. Sabas, C. W. Clyde, J. B. Baxter, C. A. Schmuttenmaer, R. H.Crabtree ; G. W. Brudvig, V. S. Batista, *J. Phys. Chem. C*. 2007, **111**, 11982–11990.

Graphical abstract: